Iron–Oxo Aggregates. Crystal Structures and Solution Characterization of 2-Hydroxy-1,3-xylylenediaminetetraacetic Acid Complexes

Bruce P. Murch,[†] Fontaine C. Bradley,[†] Paul D. Boyle,[†] Vasilios Papaefthymiou,[‡] and Lawrence Que, Jr.*[†]

Contribution from the Department of Chemistry, University of Minnesota, Minneapolis, Minnesota 55455, and Gray Freshwater Biological Institute, University of Minnesota, Navarre, Minnesota 55392. *Received March 13, 1987*

Abstract: Three iron(III) complexes of *N,N'*-2-hydroxy-5-R-1,3-xylylenebis[*N*-(carboxymethyl)glycine] (5-R-HXTA; R = CH_3, Cl) have been characterized in aqueous solution by visible, resonance Raman, NMR, and Mössbauer spectroscopy and magnetic susceptibility. The low-pH complex, $[Fe_2(5\text{-Me-HXTA})OH(H_2O)_2]$, crystallizes in the space group $C2/c$ (a = 21.074 (6), b = 10.260 (3), c = 23.931 (9) Å; β = 102.25 (3)°) and consists of two six-coordinate Fe(III) centers bridged by phenolate and hydroxide. The high-pH complex, $(C_4H_{10}N)_4[Fe_4(5\text{-Me-HXTA})_2O_2(OH)_2]$, crystallizes in the space group $P2/n$ (a = 14.465 (3), b = 11.379 (6), c = 20.530 (4) Å; β = 91.36 (2)°); the complex consists of a tetrahedron of iron(III) centers cumulatively bridged by six oxygens (two oxo, two hydroxo, and two phenoxo groups), yielding an adamantane-like Fe_4O_6 structure. These complexes retain their solid-state structures in solution on the basis of their spectroscopic properties. The intermediate-pH complex, characterized only in solution, is a tetranuclear complex derived from the dimerization of $[Fe_2(5\text{-Me-HXTA})OH(H_2O)_2]$ by the replacement of a terminal aquo ligand on each binuclear complex by an oxo group bridging the two binuclear units. Such a structure is derived from the following observations: the concentration dependence of its extinction coefficient, the presence of an Fe–O–Fe vibration in its Raman spectrum, the Curie temperature dependence of some NMR features and the anti-Curie behavior of others indicative of the presence of both strongly coupled and weakly coupled pairs of iron(III) centers, and the appearance of two Mössbauer quadrupole doublets with large and small ΔE_Q values in a 1:1 ratio. The solution behavior of the HXTA complex is contrasted to that of the corresponding *N*-(*o*-hydroxybenzyl)-*N*-(carboxymethyl)glycine complexes, which retain their mononuclear character over the pH range studied. This difference in oligomerization tendency is attributed to the difference in Lewis acidity of the iron(III) centers.

The ready hydrolysis of ferric ion at neutral pH to form insoluble hydrated oxides[1] is circumvented by nature with use of coordination chemistry to control the hydrolytic process for the transport, utilization, and storage of iron(III) in the cell.[2,3] Thus, binding sites have been evolved to stabilize mononuclear, binuclear, and polynuclear iron centers in biological systems. A variety of ligand environments can be found in mononuclear sites, including porphyrins, thiolates, and phenolates. Known binuclear sites involve either bis(μ-sulfido) bridges as in 2Fe ferredoxins[4] or (μ-oxo)bis(μ-carboxylato) bridges as in hemerythrin[5] and ribonucleotide reductase.[6] Larger metal aggregates are found in other iron–sulfur proteins[4] and ferritin, the mammalian iron-storage protein. Ferritin consists of a protein shell surrounding an iron oxide (ca. 4500 iron atoms) core.[3,7,8] The mechanisms of core nucleation and propagation have been actively investigated in recent years; these studies point to a role for functional groups in the protein shell for these processes.[9-12]

Interest in ferritin chemistry has resulted in the characterization of a number of oligomeric iron–oxo species with core compositions of Fe_3O,[13,14] Fe_4O_2,[1,15,16] $Fe_4O_2(OH)_2$,[17] $Fe_8O_2(OH)_{12}$,[18] and $Fe_{11}O_6(OH)_6$.[19] Of these complexes, the tetranuclear species show a range of core arrangements with μ_2-oxo or μ_3-oxo units. We have briefly communicated the synthesis and crystal structure of $(pyrrH)_4[Fe_4(5\text{-Me-HXTA})_2O_2(OH)_2]$,[20] which features an adamantane-like Fe_4O_6 core.[17] Herein, we describe in detail the crystal structure of this tetranuclear species and that of its binuclear parent, $[Fe_2(5\text{-Me-HXTA})OH(H_2O)_2]$. We also discuss their solution chemistry and, in particular, the mechanism of interconversion between the two complexes, which involves yet another tetranuclear species as an intermediate. Comparisons with the solution chemistry of the corresponding mononucleating ligand are also made.

Experimental Section

Synthesis. The parent HDA ligand was synthesized according to the method of Martell[21] and characterized by its NMR spectrum. The HXTA and the other HDA ligands were synthesized from the appropriate phenols, iminodiacetic acid, and formaldehyde by a modification

[†] Department of Chemistry.
[‡] Gray Freshwater Biological Institute.

(1) Flynn, C. M., Jr. *Chem. Rev.* **1984**, *84*, 31–42.
(2) Lippard, S. J. *Chem. Br.* **1986**, *16*, 222–229.
(3) Aisen, P.; Listowsky, I. *Annu. Rev. Biochem.* **1980**, *49*, 357–393.
(4) Holm, R. H.; Ibers, J. A. *Science (Washington, D.C.)* **1980**, *209*, 223–235.
(5) Stenkamp, R. E.; Sieker, L. C.; Jensen, L. H. *J. Am. Chem. Soc.* **1984**, *106*, 618–622.
(6) Sjöberg, B.-M.; Gräslund, A. *Adv. Inorg. Biochem.* **1983**, *5*, 87–110. Scarrow, R. C.; Maroney, M. J.; Palmer, S. M.; Que, L., Jr.; Salowe, S. P.; Stubbe, J. *J. Am. Chem. Soc.* **1986**, *108*, 6832–6834.
(7) Theil, E. C. *Adv. Inorg. Biochem.* **1983**, *5*, 1–38.
(8) Rice, D. W.; Ford, G. C.; White, J. L.; Smith, J. M. A.; Harrison, P. M. *Adv. Inorg. Biochem.* **1983**, *5*, 39–50.
(9) Mertz, J. R.; Theil, E. C. *J. Biol. Chem.* **1983**, *258*, 11719–11726.
(10) Sayers, D. E.; Theil, E. C.; Rennick, F. J. *J. Biol. Chem.* **1983**, *258*, 14076–14079.
(11) Chasteen, N. D.; Theil, E. C. *J. Biol. Chem.* **1982**, *257*, 7672–7677.
(12) Chasteen, N. D.; Antanaitis, B. C.; Aisen, P. *J. Biol. Chem.* **1985**, *260*, 2926–2929.
(13) Cotton, F. A.; Wilkinson, G. *Advanced Inorganic Chemistry*, 4th ed.; Wiley: New York, 1980; p 154.
(14) Gorun, S. M.; Lippard, S. J. *J. Am. Chem. Soc.* **1985**, *107*, 4568–4570.
(15) Toftlund, H.; Murray, K. S.; Zwack, P. R.; Taylor, L. F.; Anderson, O. P. *J. Chem. Soc., Chem. Commun.* **1986**, 191–192. Turtê, K. I.; Bobkova, S. A.; Kuyavskaya, B. Ya.; Ivleva, I. N.; Vekselman, M. E. *Koord. Khim.* **1985**, *11*, 1106.
(16) Jameson, D. L.; Xie, C.-L.; Hendrickson, D. N.; Potenza, J. A.; Schugar, H. J. *J. Am. Chem. Soc.* **1987**, *109*, 740–746.
(17) Murch, B. P.; Boyle, P. D.; Que, L., Jr. *J. Am. Chem. Soc.* **1985**, *107*, 6728–6729.
(18) Wieghardt, K.; Pohl, K.; Jibril, I.; Huttner, G. *Angew. Chem., Int. Ed. Engl.* **1984**, *23*, 77–78.
(19) Gorun, S.; Lippard, S. J. *Nature (London)* **1986**, *319*, 666–668.
(20) Abbreviations used: HXTA, *N,N'*-2-hydroxy-1,3-xylylenebis[*N*-(carboxymethyl)glycine]; pyrr, pyrrolidine; HDA, *N*-(2-hydroxybenzyl)-*N*-(carboxymethyl)glycine; Cl_2HDA, *N*-(4,6-dichloro-2-hydroxybenzyl)-*N*-(carboxymethyl)glycine; Bu_2HDA, *N*-(4,6-di-*tert*-butyl-2-hydroxybenzyl)-*N*-(carboxymethyl)glycine; IDA, *N*-(carboxymethyl)glycine; $(sal)_3$trien, trisalicylidene triethylenetetramine; NTA, *N,N*-bis(carboxymethyl)glycine; DBC, 3,5-di-*tert*-butylcatechol; phen, 1,10-phenanthroline; EDTA, *N,N'*-ethylene[bis(carboxymethyl)glycine)]; HEDTA, *N,N'*-ethylene-*N*-(2-hydroxyethyl)glycine-*N*-(carboxymethyl)glycine; Cl(dipic), 4-chloropyridine-2,6-dicarboxylic acid; $HB(pz)_3$, hydrotris(pyrazolyl)borate; tacn, 1,4,7-triazacyclononane; *N*-Prsal, *N*-propylsalicylideneamine.

0002-7863/87/1509-7993$01.50/0 © 1987 American Chemical Society

of the procedure of Schwarzenbach.[22] The syntheses of Na_2Cl_2HDA and Na_2Bu_2HDA have been previously reported.[26] Na_2-5-Me-HDA was synthesized following a similar procedure; it was then neutralized with 2 equiv of HCl and the resulting acid slowly crystallized from water. For Na_3-5-Me-HXTA and Na_3-5-Cl-HXTA, the sodium phenolate (10 mmol) was reacted with 2 equiv of the monosodium salt of iminodiacetic acid and 2 equiv of formaldehyde at 0 °C in water (8 mL) for 30 min, followed by 12 h of stirring at room temperature and then heating at 60–70 °C for 3 h. The ligands were then isolated by dilution with methanol to yield the trisodium salts. The identities of the ligands were confirmed by NMR spectroscopy in D_2O. Na_2Cl_2HDA: δ 3.60 (s, 4 H), 4.21 (s, 2 H), 7.09 (d, J = 2.6 Hz, 1 H), 7.40 (d, J = 2.6 Hz, 1 H). Na_2Bu_2HDA: δ 1.23 (s, 9 H), 1.37 (s, 9 H), 3.22 (s, 4 H), 3.82 (s, 2 H), 7.06 (d, J = 2.5 Hz, 1 H), 7.33 (d, J = 2.5 Hz, 1 H). Na_2-5-Me-HDA: δ 2.22 (s, 3 H), 3.2 (s, 4 H), 3.7 (s, 2 H), 6.55 (d, J = 9 Hz, 1 H), 6.9 (d, J = 9 Hz, 1 H), 6.95 (s, 1 H). Na_3-5-Me-HXTA: δ 2.17 (s, 3 H), 3.48 (s, 8 H), 4.09 (s, 4 H), 7.02 (s, 2 H). Na_3-5-Cl-HXTA: δ 3.58 (s, 8 H), 4.19 (s, 4 H), 7.24 (s, 2 H).

Deuteriated derivatives of Na_3-5-Me-HXTA were obtained from appropriate starting materials. The meta-deuteriated derivative was synthesized from p-cresol-d_5.[23] NMR integration of the resulting compound showed approximately 75% deuterium incorporation at the meta positions of the phenol. The carboxymethylene-deuteriated derivative was prepared from deuteriated iminodiacetic acid via a modification of a procedure by Keyes and Legg.[24] $K[Co(IDA)_2]$[25] was heated at 40 °C in carbonate buffer, pH 9.6, dissolved in D_2O for 3 weeks. The cobalt was stripped from the ligand by adding 7.5 equiv of NaCN and refluxing for 10 min. Acidification removed excess cyanide. Due to the difficulty of separating the deuteriated IDA from $[Co(CN)_6]^{3-}$ the crude reaction mixture was used to prepare the deuteriated 5-Me-HXTA ligand; NMR integration of the resulting compound indicated >90% incorporation of deuterium in the carboxymethylene positions.

The aquo complexes of [Fe(Cl_2HDA)] and [Fe(Bu_2HDA)] were prepared from the reaction of a ferric salt with the sodium salt of the appropriate ligand and 1 equiv of base in water. Needles were obtained from the reaction solutions (pH 2.5) and recrystallized from water or methanol to yield analytically pure samples of [Fe(Cl_2HDA)(H_2O)$_2$] and [Fe(Bu_2HDA)(CH_3OH)$_2$], respectively.[26] [Fe(HDA)] and [Fe(5-Me-HDA)] complexes could not be isolated without contaminating salts and were thus generated in situ by the stoichiometric addition of ferric salts to solutions of the ligands for the spectral titrations.

[Fe_2(5-R-HXTA)OH(H_2O)$_2$] complexes (R = Me, Cl) were prepared by the following procedure. Addition of 1 equiv of $Fe(NO_3)_3 \cdot 9H_2O$ to an aqueous solution (0.05–0.10 M) of Na_3HXTA lowers the solution pH to 2–3. Raising the pH to 8–9 (2.5–3 equiv of NaOH) followed by the addition of another 1 equiv of iron and filtering yields crystalline product upon standing overnight in 40–70% yield. Anal. Calcd for [Fe_2(5-Me-HXTA)OH(H_2O)$_2$]·2.5H_2O ($C_{17}H_{27}Fe_2N_2O_{14.5}$): C, 33.85; H, 4.51; N, 4.64. Found: C, 32.93; H, 4.63; N, 4.54. Anal. Calcd for [Fe_2(5-Cl-HXTA)OH(H_2O)$_2$]·3H_2O ($C_{16}H_{25}ClFe_2N_2O_{15}$): C, 30.38; H, 3.98; N, 4.42. Found: C, 30.20; H, 4.15; N, 4.29. Crystals of X-ray diffraction quality of [Fe_2(5-Me-HXTA)OH(H_2O)$_2$] were obtained by recrystallization from hot water with slow cooling.

The tetranuclear complex (pyrrH)$_4$[Fe_4(5-Me-HXTA)$_2O_2$(OH)$_2$] was prepared by dissolving 0.3 g of [Fe_2(5-Me-HXTA)OH(H_2O)$_2$] in 10 mL of methanol with at least a fourfold excess of pyrrolidine. Evaporation to about 2 mL, followed by filtration and slow vapor diffusion of acetone into the solution, afforded crystals suitable for X-ray diffraction studies. Anal. Calcd for (pyrrH)$_4$[Fe_4(5-Me-HXTA)$_2O_2$(OH)$_2$]·2CH_3OH ($C_{52}H_{84}Fe_4N_8O_{24}$): C, 43.71; H, 5.93; N, 7.84. Found: C, 43.71; H, 6.06; N, 7.88.

Caution! One of us developed an allergy to the HXTA ligands and complexes. Care should be exercised to avoid contact with the compounds.

Methods. X-ray diffraction studies were performed at the crystallography facility of the University of Minnesota Chemistry Department on an Enraf-Nonius CAD4 diffractometer at 298 K. Both crystals were mounted in capillary tubes containing mother liquor and sealed with epoxy. The iron atoms were located by direct methods for the tetranuclear complex and by Patterson maps for the binuclear complex. The other atoms for the two structures were then located by Fourier and direct methods and refined anisotropically.

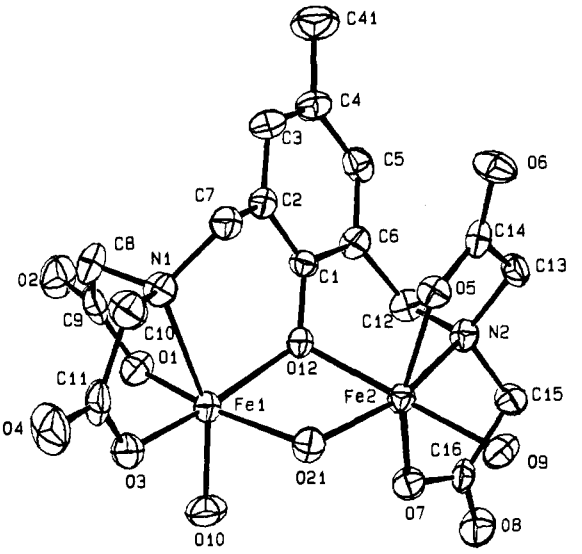

Figure 1. Structure of [Fe_2(5-Me-HXTA)OH(H_2O)$_2$] showing 50% probability ellipsoids and atom-labeling scheme. Hydrogen atoms have been omitted for clarity.

UV–visible spectra were recorded on an HP 8451A diode array spectrometer. Resonance Raman spectra were obtained on a Spex 1403 spectrometer interfaces with a Spex Datamate with the lines of a Spectra Physics 171 argon ion laser or a Spectra Physics 375B dye laser (Rhodamine 6G) pumped by the argon ion laser. Spectra were obtained at room temperature with a spinning quartz cell with the incidient laser beam 90° relative to the scattered light collected. Raman frequencies are referenced against a 0.1 M sulfate internal standard.

NMR spectra were obtained on a Nicolet NT-300 NMR spectrometer operating at 300 MHz with a 100 000-Hz spectral width and a 90° acquisition pulse. For the variable-temperature experiments, temperature calibration was accomplished with methanol/HCl solutions at low temperature and ethylene glycol at elevated temperatures.[27] Complexes with concentrations of 2–20 mM required 1000–4000 scans to yield spectra of adequate signal-to-noise ratios.

Mössbauer spectra were obtained in Professor Eckard Münck's laboratory as previously described.[28a] Magnetic susceptibility measurements were made in vacuo on solid samples at room temperature and three arbitrary fields with use of a Faraday balance calibrated with Hg[Co(SCN)$_4$]; the magnetic moments obtained were found to be field independent. Diamagnetic corrections were estimated by Pascal's constants.[28b]

Variable-temperature solid-state magnetic susceptibility measurements were performed by R. L. Rardin of the Department of Chemistry, Massachusetts Institute of Technology at the Francis Bitter National Magnet Laboratory. Data for 29.4 mg of powdered, analytically pure [Fe_2(5-Me-HXTA)OH(H_2O)$_2$]·2H_2O were measured at 10 kG with a SHE Model 905 SQUID-type magnetometer over a temperature range of 6.0–300 K. Data for the Si–Al alloy sample holder used in the experiment were also measured at the same temperatures to allow for accurate correction of the paramagnetic contribution of the sample holder to the total susceptibility. Pascal's constants[28b] were used to calculate a diamagnetic correction of -282.0×10^{-6} emu G^{-1} mol^{-1} for the complex. The data were fit to the equation

$$\chi_M = \frac{(1-p)C(2e^{2x} + 10e^{6x} + 28e^{12x} + 60e^{20x} + 110e^{30x})}{1 + 3e^{2x} + 5e^{6x} + 7e^{12x} + 9e^{20x} + 11e^{30x}} + 4.4p/T$$

where $C = Ng^2\mu_B^2/kT$, $x = J/kT$, and p is the mole fraction of a paramagnetic impurity. The equation is based on a theoretical expression for the temperature-dependent susceptibility of a coupled binuclear system derived from the general isotropic exchange Hamiltonian, $H = -2JS_1 \cdot S_2$, where $S_1 = S_2 = {}^5/_2$; a term correcting for a paramagnetic

(21) Harris, W. R.; Motekaitis, R. J.; Martell, A. E. *Inorg. Chem.* **1975**, *14*, 974–978.
(22) Schwarzenbach, G.; Anderegg, G.; Sallmann, R. *Helv. Chim. Acta* **1952**, *35*, 1785–1792.
(23) Jakobsen, R. J. *Spectrochim. Acta* **1965**, *21*, 433–442.
(24) Keyes, W. E.; Legg, J. I. *J. Am. Chem. Soc.* **1976**, *98*, 4970–4975.
(25) Hidaka, J.; Shimura, Y.; Tsuchida, R. *Bull. Chem. Soc. Jpn.* **1962**, *35*, 567–571.
(26) Que, L., Jr.; Kolanczyk, R. C.; White, L. S. *J. Am. Chem. Soc.* **1987**, *109*, 5373–5380.
(27) Van Geet, A. L. *Anal. Chem.* **1970**, *42*, 679–680.
(28) (a) Zimmermann, R.; Münck, E.; Brill, W. J.; Shah, V. K.; Henzl, M. T.; Rawlings, J.; Orme-Johnson, W. H. *Biochim. Biophys. Acta* **1978**, *537*, 185–207. (b) Carlin, R. L. *Magnetochemistry*; Springer-Verlag: New York, 1986; p 3. O'Connor, C. J. *Prog. Inorg. Chem.* **1979**, *29*, 204–283.

Table I. Crystallographic Data for $[Fe_2(5\text{-Me-HXTA})OH(H_2O)_2]\cdot 4H_2O$ and $(pyrrH)_4[Fe_4(5\text{-Me-HXTA})_2O_2(OH)_2]\cdot 5CH_3OH$

formula	$C_{17}H_{30}Fe_2N_2O_{16}$	$C_{55}H_{96}Fe_4N_8O_{27}$
MW	630.13	1524.64
space grp	$C2/c$	$P2/n$
a, Å	21.074 (6)	14.465 (3)
b, Å	10.260 (3)	11.379 (6)
c, Å	23.931 (9)	20.530 (4)
α, deg	90.0	90.0
β, deg	102.25 (3)	91.36 (2)
γ, deg	90.0	90.0
V, Å^3	5056 (5)	3378 (3)
Z	8	2
D_{calcd}, g/cm^3	1.655	1.499
radiat used (λ, Å)	Mo Kα (0.71073)	Mo Kα (0.71073)
max $(\sin\theta)/\lambda$	0.57	0.57
cryst size, mm^3	0.3 × 0.2 × 0.2	0.3 × 0.3 × 0.2
μ, cm^{-1}	12.222	9.295
no. of reflcns measd	3971	5276
reflcns used[a]	2502 $[(F_o)^2 \geq 1\sigma(F_o)^2]$	3303 $[(F_o)^2 \geq 2\sigma(F_o)^2]$
no. of variables used	318	398
R[b]	0.054	0.054
R_w[b]	0.058	0.062
GOF[b]	1.627	1.824
p[a]	0.04	0.04

[a] The intensity data were processed as described in: *CAD 4 and SDP-PLUS User's Manual*; B. A. Frenz & Associates: College Station, TX, 1982. The net intensity $I = [K(NPI)](C - 2B)$, where K = 20.1166 (attenuator factor), NPI = ratio of fastest possible scan rate to scan rate for the measurement, C = total count, and B = total background count. The standard deviation in the net intensity is given by $[\sigma(I)]^2 = (k/NPI)^2[C + 4B + (pI)^2]$ where p is a factor used to downweight intense reflections. The observed structure factor amplitude F_o is given by $F_o = (I/Lp)^{1/2}$, where Lp = Lorentz and polarization factors. The $\sigma(I)$'s were converted to the estimated errors in the relative structure factors $\sigma(F_o)$ by $\sigma(F_o) = {}^1/_2[\sigma(I)/I]F_o$. [b] The function minimized was $\sum w(|F_o| - |F_c|)^2$, where $w = 1/[\sigma(F_o)]^2$. The unweighted and weighted residuals are defined as $R = (||F_o| - |F_c||)/\sum|F_o|$ and $R_w = [(\sum w(|F_o| - |F_c|)^2/(\sum w|F_o|)^2]^{1/2}$. The error is an observation of unit weight. GOF is $[\sum w(|F_o| - |F_c|)^2/(NO - NV)]^{1/2}$, where NO and NV are the number of observations and variables, respectively.

impurity has also been added. The absence of ferromagnetic impurities in the sample was confirmed by the field independence of the susceptibility at 77 and 150 K in fields ranging from 0.5 to 50 kG.

Results and Discussion

Crystal Structures of $[Fe_2(5\text{-Me-HXTA})OH(H_2O)_2]$ and $(pyrrH)_4[Fe_4(5\text{-Me-HXTA})_2O_2(OH)_2]$. The functional groups of the binucleating 5-Me-HXTA ligand provide a coordination environment with high affinity for iron(III). Two complexes have been crystallized from aqueous solutions; under acidic conditions, a binuclear species, $[Fe_2(5\text{-Me-HXTA})OH(H_2O)_2]$, is obtained, while a tetranuclear species, $(pyrrH)_4[Fe_4(5\text{-Me-HXTA})_2O_2(OH)_2]$, is isolated under basic conditions. The crystallographic data for the two complexes are summarized in Table I.

$[Fe_2(5\text{-Me-HXTA})OH(H_2O)_2]$ crystallizes in the monoclinic space group $C2/c$. The structure is shown in Figure 1 together with the numbering scheme for the molecule. Atomic coordinates for the non-hydrogen atoms of the complex and selected bond distances and bond angles are given in Tables II and III, respectively. Atomic coordinates for the hydrogen atoms and the solvent molecules in the crystal, thermal factors, and appropriate least-squares planes for the complex are found in Tables S1–S3, respectively (supplementary material).

The structure of the complex consists of two iron centers in distorted octahedra joined along a common edge by the bridging phenolate (O12) and hydroxide (O21), with both bridging atoms somewhat asymmetrically disposed between the iron atoms. The coordination sphere about each iron is completed by two carboxylates, a tertiary nitrogen, and a water molecule. The average iron–hydroxide bond is 1.96 (2) Å long and compares well with

Table II. Atomic Coordinates for the Non-Hydrogen Atoms of $[Fe_2(5\text{-Me-HXTA})OH(H_2O)_2]$

atom	x	y	z	B, Å^2
Fe1	−0.06755 (4)	0.1609 (1)	0.14665 (4)	2.07 (2)
Fe2	−0.18382 (4)	0.24335 (9)	0.20189 (4)	1.82 (2)
O1	−0.0628 (2)	0.1801 (5)	0.0658 (2)	2.7 (1)
O2	−0.0707 (2)	0.0904 (6)	−0.0194 (2)	3.7 (1)
O3	0.0154 (2)	0.0767 (5)	0.1811 (2)	2.7 (1)
O4	0.0687 (2)	−0.1059 (6)	0.2100 (2)	4.1 (1)
O5	−0.2394 (2)	0.0879 (4)	0.1987 (2)	2.0 (1)
O6	−0.3358 (2)	−0.0042 (5)	0.1665 (2)	2.9 (1)
O7	−0.1662 (2)	0.4321 (4)	0.1964 (2)	2.4 (1)
O8	−0.2091 (2)	0.6317 (4)	0.1891 (2)	3.2 (1)
O9	−0.2000 (2)	0.2749 (4)	0.2807 (2)	2.7 (1)
O10	−0.0288 (2)	0.3404 (5)	0.1545 (2)	3.3 (1)
O12	−0.1638 (2)	0.1880 (4)	0.1265 (2)	2.0 (1)
O21	−0.0949 (2)	0.1808 (5)	0.2204 (2)	2.3 (1)
N1	−0.0853 (3)	−0.0432 (5)	0.1168 (2)	2.3 (1)
N2	−0.2768 (2)	0.3172 (5)	0.1495 (2)	2.0 (1)
C1	−0.2099 (3)	0.1269 (6)	0.0868 (3)	1.9 (1)
C2	−0.2039 (3)	−0.0064 (7)	0.0758 (3)	2.3 (2)
C3	−0.2519 (3)	−0.0622 (7)	0.0339 (3)	3.0 (2)
C4	−0.3056 (3)	0.0062 (8)	0.0058 (3)	2.9 (2)
C5	−0.3135 (3)	0.1338 (7)	0.0225 (3)	2.4 (2)
C6	−0.2662 (3)	0.1943 (7)	0.0635 (3)	2.2 (1)
C7	−0.1536 (3)	−0.0861 (7)	0.1140 (3)	2.6 (2)
C8	−0.0688 (3)	−0.0496 (8)	0.0594 (3)	3.3 (2)
C9	−0.0681 (3)	0.0834 (8)	0.0319 (3)	2.8 (2)
C10	−0.0401 (3)	−0.1245 (7)	0.1581 (4)	3.2 (2)
C11	0.0202 (3)	−0.0488 (7)	0.1847 (3)	2.9 (2)
C12	−0.2751 (3)	0.3271 (7)	0.0876 (3)	2.5 (2)
C13	−0.3283 (3)	0.2269 (7)	0.1594 (3)	2.2 (1)
C14	−0.3002 (3)	0.0924 (7)	0.1743 (3)	2.1 (1)
C15	−0.2823 (3)	0.4507 (6)	0.1719 (3)	2.3 (2)
C16	−0.2151 (3)	0.5119 (7)	0.1863 (3)	2.1 (1)
C41	−0.3565 (4)	−0.0561 (9)	−0.0407 (4)	4.6 (2)

such bonds in other hydroxy-bridged iron dimers.[29-31] The average iron–phenolate bond length, 2.01 (1) Å, is shorter than that found for the bridging phenolate in $Fe_2(sal)_3trien(OMe)Cl_2$[32] and $Fe_2(sal)_3trien(OH)Cl_2$[31] (2.06 (2) Å); the longer bond length for the $(sal)_3trien$ complexes probably reflects the diminshed Lewis acidity of the iron center in these complexes due to the presence of strong iron–terminal phenolate bonds (Fe–O 1.89 Å).

The Fe–N and Fe–O (carboxylate) bond lengths for the binuclear complex, averaging 2.22 and 1.97 Å, respectively, are comparable to those of other complexes. Examples of Fe–N (tertiary amine) bonds in similar complexes are the following: $[Fe(NTA)DBC]^{2-}$, 2.224 Å;[33] $Li[Fe(EDTA)H_2O]$, 2.325 Å;[34] $[Fe(HEDTA)]_2O^{2-}$, 2.25 Å.[35] Examples of Fe–O (carboxylate) bonds are the following $[Fe(NTA)DBC]^{2-}$, 2.025 Å;[33] $Li[Fe(EDTA)H_2O]$, 1.969 and 2.119 Å;[34] $[Fe(HEDTA)]_2O^{2-}$, 2.03 Å.[35] The Fe–OH_2 bonds, averaging 2.010 Å, are somewhat shorter than those in $[Fe_2(Cl(dipic))_2(H_2O)_4O]$, 2.056 Å,[36] and the seven-coordinate $Li[Fe(EDTA)H_2O]$, 2.106 Å.[34] The iron–iron separation is 3.137 (1) Å as found in similarly bridged complexes.[31,32] The iron–iron vector intersects the phenolate plane at a 45° angle, with Fe1 and Fe2 lying −0.90 and 0.60 Å out of the phenolate plane, respectively.

(29) Ou, C. C.; Wollman, R. G.; Hendrickson, D. N.; Potenza, J. A.; Schugar, H. J. *J. Am. Chem. Soc.* **1978**, *100*, 4717–4724.
(30) Armstrong, W. H.; Lippard, S. J. *J. Am. Chem. Soc.* **1984**, *106*, 4632–4633.
(31) Chiari, B.; Piovesana, O.; Tarantelli, T.; Zanazzi, P. F. *Inorg. Chem.* **1983**, *22*, 2781–2784.
(32) Chiari, B.; Piovesana, O.; Tarantelli, T.; Zanazzi, P. F. *Inorg. Chem.* **1982**, *21*, 2444–2448.
(33) White, L. S.; Nilsson, P. V.; Pignolet, L. H.; Que, L., Jr. *J. Am. Chem. Soc.* **1984**, *106*, 8312–8313.
(34) Hamor, M. J.; Hamor, T. A.; Hoard, J. L. *Inorg. Chem.* **1964**, *3*, 34–43.
(35) Lippard, S. J.; Schugar, H. J.; Walling, C. *Inorg. Chem.* **1967**, *6*, 1825–1831.
(36) Ou, C. C.; Wollman, R. G.; Hendrickson, D. N.; Potenza, J. A. Schugar, H. J. *J. Am. Chem. Soc.* **1978**, *100*, 4717–4724.

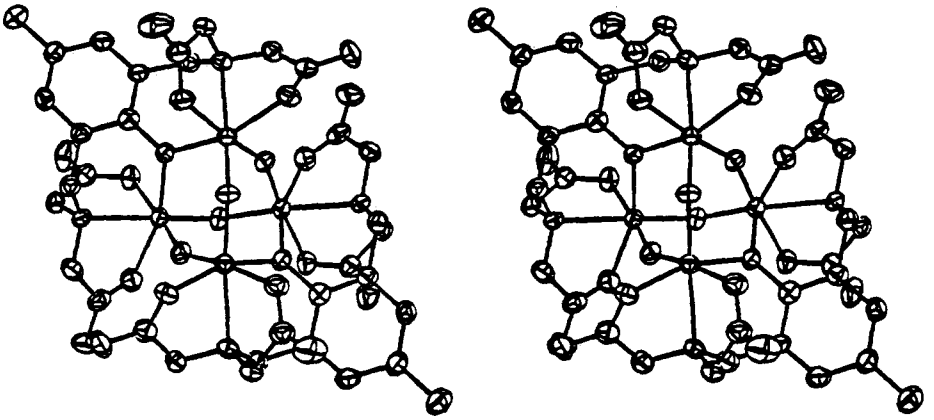

Figure 2. Stereoview of the complex $[Fe_4(5\text{-Me-HXTA})_2O_2(OH)_2]^{4-}$.

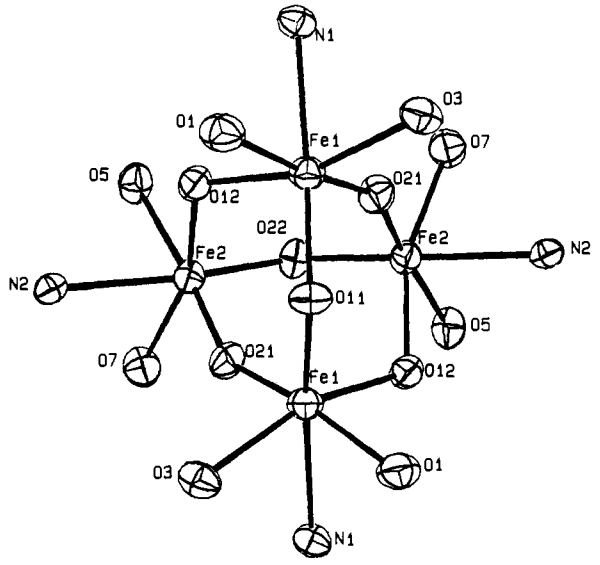

Figure 3. Structure of the $Fe_4N_4O_{14}$ core of $[Fe_4(5\text{-Me-HXTA})_2O_2(OH)_2]^{4-}$ showing 50% probability ellipsoids and atom-labeling scheme.

The geometric arrangement of the ligands around the two irons differs. On Fe1, the two carboxylates occupy cis positions and are each trans to the bridging atoms. On Fe2, the carboxylates are trans to each other, perpendicular to the approximate plane of the iron core (defined by Fe1–O12–Fe2–O21). It is not clear why the complex chose to crystallize in this particular configuration, since several other configurations can be accommodated by the structural requirements. However, the crystal form of the complex has been observed to vary depending on the solvent of crystallization;[37] this may be due either to the incorporation of different solvent molecules into the crystal lattice or to the selection of a different isomer by crystal-packing forces.

The distortion of the octahedral geometry around each iron is displayed in the acute O12–Fe–O21 angles for Fe1 and Fe2 (74.2 and 74.7°, respectively), required by the diamond geometry of the core. The N–Fe–O_2C angles are also small on each iron, averaging 78.5 (9)°. The coordinating atoms perpendicular to the plane of the iron core lean away from the core, demonstrated by the two largest angles on each iron, O21–Fe1–N1 (108.9°) and O21–Fe2–O5 (106.2°). In addition, the two three-atom planes defined by the core, Fe1–O12–O21 and Fe2–O12–O21, intersect at an angle of 166°.

$(PyrrH)_4[Fe_4(HXTA)_2O_2(OH)_2]$ crystallizes in the space group $P2/n$. A stereoview of the tetraanion is shown in Figure 2, while the Fe_4O_6 core is shown in Figure 3. The atom-labeling scheme for the ligand follows that of $[Fe_2(5\text{-Me-HXTA})OH(H_2O)_2]$, and that for the core is detailed in Figure 3. A view of the entire molecule showing cation–anion contacts can be found in Figure S1 (supplementary material). Atomic coordinates for the nonhydrogen atoms of the complex and selected bond distances and bond angles are given in Tables IV and V, respectively. Atomic coordinates for the hydrogen atoms and the solvent molecules in the crystal, thermal factors, and appropriate least-squares planes

(37) In the crystal studied, positions for five water molecules were identified in the lattice; three had partial occupancies, for a total of 3.98 (6) molecules per unit cell.

Table III. Selected Bond Lengths (Å) and Bond Angles (deg) for $[Fe_2HXTA(OH)(H_2O)_2]\cdot 5H_2O$

Bond Lengths			
Fe1–O12	2.002 (3)	Fe2–O12	2.019 (3)
Fe1–O21	1.979 (4)	Fe2–O21	1.940 (4)
Fe1–O1	1.968 (4)	Fe2–O5	1.971 (4)
Fe1–O3	1.967 (4)	Fe2–O7	1.982 (4)
Fe1–O10	2.008 (4)	Fe2–O9	2.012 (4)
Fe1–N1	2.218 (5)	Fe2–N2	2.222 (4)
O1–C9	1.272 (7)	O12–C1	1.360 (6)
O3–C11	1.293 (7)	C1–C2	1.404 (8)
O5–C14	1.291 (6)	C2–C3	1.389 (8)
O7–C16	1.298 (6)	C3–C4	1.379 (8)
N1–C7	1.494 (7)	C4–C5	1.389 (8)
N1–C8	1.490 (7)	C5–C6	1.388 (8)
N1–C10	1.476 (7)	C6–C1	1.383 (7)
O2–C9	1.220 (7)	C4–C41	1.513 (8)
O4–C11	1.222 (7)	C2–C7	1.488 (8)
O6–C14	1.233 (6)	C6–C12	1.507 (8)
O8–C16	1.236 (6)	C8–C9	1.515 (9)
N2–C12	1.494 (7)	C10–C11	1.510 (9)
N2–C13	1.485 (7)	C13–C14	1.514 (7)
N2–C15	1.483 (7)	C15–C16	1.521 (7)
Bond Angles			
Fe1–O12–Fe2	102.56 (6)	Fe1–O21–Fe2	106.34 (17)
O12–Fe1–O21	74.22 (15)	O12–Fe2–O21	74.66 (15)
O1–Fe1–O12	90.55 (16)	O5–Fe2–O12	8.46 (15)
O1–Fe1–O21	161.94 (16)	O5–Fe2–O21	106.19 (16)
O1–Fe1–O3	103.30 (17)	O5–Fe2–O7	155.03 (15)
O1–Fe1–O10	84.02 (16)	O5–Fe2–O9	87.07 (15)
O1–Fe1–N1	79.56 (17)	O5–Fe2–N2	78.94 (15)
O3–Fe1–O10	93.17 (17)	O7–Fe2–O9	88.64 (15)
O3–Fe1–O12	157.92 (16)	O7–Fe2–O12	97.93 (15)
O3–Fe1–O21	94.19 (16)	O7–Fe2–O21	98.78 (16)
O3–Fe1–N1	78.13 (16)	O7–Fe2–N2	77.57 (16)
O10–Fe1–O12	105.46 (16)	O9–Fe2–O12	172.48 (15)
O10–Fe1–O21	90.64 (16)	O9–Fe2–O21	100.81 (15)
O10–Fe1–N1	159.02 (17)	O9–Fe2–N2	99.72 (16)
O12–Fe1–N1	87.71 (16)	O12–Fe2–N2	85.34 (15)
O21–Fe1–N1	108.86 (17)	O21–Fe2–N2	159.05 (16)
Fe1–O12–C1	129.88 (32)	Fe2–O12–C1	120.02 (31)
Fe1–O1–C9	122.18 (40)	Fe2–O5–C14	120.92 (33)
Fe1–O3–C11	121.02 (37)	Fe2–O7–C16	188.41 (34)
Fe1–N1–C7	112.78 (33)	Fe2–N2–C12	112.25 (31)
Fe1–N1–C8	106.36 (35)	Fe2–N2–C13	106.55 (33)
Fe1–N1–C10	106.10 (34)	Fe2–N2–C15	103.84 (32)
C7–N1–C8	110.92 (45)	C12–N2–C13	111.89 (43)
C7–N1–C10	110.08 (44)	C12–N2–C15	108.34 (44)
C8–N1–C10	110.45 (43)	C13–N2–C15	113.71 (40)

Table IV. Atomic Coordinates for Non-Hydrogen Atoms of $(pyrrH)_4[Fe_4(5\text{-Me-HXTA})_2O_2(OH)_2]$

atom	*x*	*y*	*z*	*B*, Å²
Fe1	0.63943 (6)	0.29814 (8)	0.21714 (4)	2.21 (2)
Fe2	0.71700 (6)	0.07061 (8)	0.32972 (4)	2.19 (2)
O1	0.5611 (3)	0.4302 (4)	0.2615 (2)	3.00 (9)
O2	0.4292 (3)	0.5291 (5)	0.2626 (3)	4.9 (1)
O3	0.6196 (3)	0.3913 (4)	0.1281 (2)	2.74 (9)
O4	0.5784 (3)	0.3424 (4)	0.0260 (2)	3.8 (1)
O5	0.6107 (3)	−0.0518 (4)	0.3421 (2)	2.80 (9)
O6	0.5157 (3)	−0.1384 (4)	0.4117 (2)	4.4 (1)
O7	0.8016 (3)	−0.0302 (4)	0.3941 (2)	3.1 (1)
O8	0.8875 (3)	−0.0037 (5)	0.4852 (2)	4.6 (1)
O11	0.750	0.3857 (5)	0.250	2.6 (1)
O12	0.8835 (2)	0.1881 (4)	0.2044 (2)	2.41 (9)
O21	0.6962 (3)	0.1823 (4)	0.1746 (2)	2.61 (9)
O22	0.750	−0.0178 (5)	0.250	2.6 (1)
N1	0.4954 (3)	0.2582 (4)	0.1824 (2)	2.2 (1)
N2	0.6699 (3)	0.1115 (4)	0.4300 (2)	2.1 (1)
C1	0.5325 (4)	0.1938 (5)	0.3251 (3)	2.4 (1)
C2	0.4513 (4)	0.1754 (6)	0.2880 (3)	2.4 (1)
C3	0.3685 (4)	0.1809 (6)	0.3181 (3)	3.2 (2)
C4	0.3613 (4)	0.2009 (7)	0.3845 (3)	3.4 (2)
C5	0.4427 (4)	0.2151 (6)	0.4205 (3)	2.8 (1)
C6	0.5287 (4)	0.2128 (6)	0.3919 (3)	2.4 (1)
C7	0.4597 (4)	0.1521 (6)	0.2160 (3)	2.7 (1)
C8	0.4369 (4)	0.3633 (6)	0.1932 (3)	2.8 (1)
C9	0.4778 (4)	0.4484 (6)	0.2434 (3)	3.1 (1)
C10	0.5084 (4)	0.2389 (6)	0.1120 (3)	2.7 (1)
C11	0.5735 (4)	0.3329 (6)	0.0864 (3)	2.8 (1)
C12	0.6170 (4)	0.2231 (6)	0.4316 (3)	2.7 (1)
C13	0.6141 (4)	0.0124 (6)	0.4529 (3)	2.6 (1)
C14	0.5750 (4)	−0.0637 (6)	0.3979 (3)	2.9 (1)
C15	0.7564 (4)	0.1200 (6)	0.4680 (3)	3.0 (1)
C16	0.8208 (4)	0.0196 (6)	0.4472 (3)	3.0 (1)
C41	0.2679 (5)	0.2053 (8)	0.4162 (4)	5.0 (2)
N1P	0.5168 (4)	0.8063 (6)	0.0599 (3)	4.4 (1)
C2P	0.5853 (6)	0.7187 (8)	0.0833 (5)	6.6 (2)
C3P	0.570 (1)	0.704 (1)	0.1513 (6)	16.3 (5)
C4P	0.499 (1)	0.787 (1)	0.1717 (5)	14.1 (5)
C5P	0.4604 (7)	0.8444 (9)	0.1159 (4)	6.6 (3)
N6P	0.5383 (5)	0.6501 (6)	0.3523 (3)	5.3 (2)
C7P	0.6396 (7)	0.6473 (9)	0.3415 (5)	7.7 (3)
C8P	0.6765 (9)	0.571 (2)	0.3939 (6)	15.0 (6)
C9P	0.612 (1)	0.550 (1)	0.4404 (6)	12.0 (4)
C10P	0.5198 (9)	0.5715 (9)	0.4084 (5)	8.9 (3)

for the complex are found in Tables S4–S6, respectively (supplementary material).

The iron core consists of a tetrahedron of irons bridged on each of the six edges by oxygen ligands, provided by two phenolato (O12), two hydroxo (O11, O22), and two oxo (O21) groups. One crystallographically imposed C_2 axis passes through the hydroxo bridges, resulting in four unique iron–iron distances. The iron–iron separation is 3.631 (1) Å across the phenolate, 3.469 (1) Å across the oxo bridges, and 3.442 (1) and 3.432 (1) Å across the two hydroxo bridges. The hydroxo and phenolato bridges form similar Fe–O–Fe angles, 119.5° and 121.6°, respectively; the iron–oxo–iron angles are much wider (151.2°) to offset the short iron–oxo bond distance while maintaining the iron–iron separation.

There are two approximate C_2 axes passing through oxo oxygens and phenolato oxygens, respectively, in addition to the crystallographic C_2 axis. Thus, the geometries around each iron are the same for all four irons. The iron–oxo bonds, Fe–O21, are 1.791 (1) Å long and comparable in length with other such bonds.[38-40] The iron–phenolate bonds, Fe–O12, average 2.079 (5) Å and are trans to the iron–carboxylate bonds, Fe1–O3 and Fe2–O7. These bonds are slightly longer (2.122 (5) Å) than the other two iron–carboxylate bonds (2.098 (4) Å), which are trans to the iron–oxo bonds; this lack of an oxo trans effect contrasts observations on nearly all other oxo-bridged structures where the bond trans to the oxo group is lengthened.[38] The iron–hydroxo bonds (1.989 Å), Fe–O11 and Fe–O22, are trans to the long iron–tertiary amine bonds (2.233 (1) Å).

Each iron is in a distorted octahedron. The distortion is displayed in acute angles of 73.8° and 77.3° for the O3–Fe1–N1 and O7–Fe2–N2 angles. The largest angle on either iron is displayed by the O12–Fe1–O11 or O12–Fe2–O22 angles (101.8 (1.3)°). The axial O11–Fe1–N1 or O22–Fe2–N2 axis (161.4 (1)°) leans away from the core, and the O3–Fe1–O12 and O7–Fe2–O12 (161.3 (3)°) axes distort away from the bridging hydroxides. The standard deviation from octahedral angles is 8.1°. As with $[Fe_2(5\text{-Me-HXTA})OH(H_2O)_2]$, the Fe1–Fe2 vector intersects the plane of the phenolate ring at a 45° angle.

The availability of the above two structures provides an opportunity to examine the effects of core size on M–L bond lengths. With the introduction of the short iron–oxo bonds in the tetranuclear complex, there is a dramatic lengthening of the other bonds from the binuclear to the tetranuclear complex. The iron–hydroxide bonds lengthen by 0.03 Å, while the iron–phenolate bonds increase by 0.08 Å. The iron–carboxylate bonds, which average 0.14 Å longer, are the longest of any six-coordinate iron(III)–carboxylate complex known; they approach lengths found

Table V. Selected Bond Lengths (Å) and Bond Angles (deg) for $[Fe_4HXTA_2(O)_2(OH)_2]^{4-}$

Bond Lengths			
Fe1–O1	2.102 (3)	Fe2–O5	2.095 (3)
Fe1–O3	2.127 (3)	Fe2–O7	2.117 (3)
Fe1–O11	1.989 (2)	Fe2–O22	1.989 (2)
Fe1–O12	2.074 (3)	Fe2–O12	2.084 (3)
Fe1–O21	1.792 (3)	Fe2–O21	1.790 (3)
Fe1–N1	2.233 (4)	Fe2–N2	2.233 (4)
O1–C9	1.269 (5)	O2–C9	1.228 (6)
O3–C11	1.262 (6)	O4–C11	1.247 (6)
O5–C14	1.274 (2)	O6–C14	1.245 (6)
O7–C16	1.253 (6)	O8–C16	1.255 (6)
N1–C7	1.490 (6)	N2–C12	1.484 (6)
N1–C8	1.484 (6)	N2–C13	1.470 (6)
N1–C10	1.477 (6)	N2–C15	1.462 (5)
O12–C1	1.371 (5)	C2–C3	1.362 (6)
C1–C2	1.399 (6)	C4–C5	1.385 (6)
C3–C4	1.389 (6)	C4–C41	1.514 (7)
C5–C6	1.389 (6)	C6–C1	1.390 (6)
C2–C7	1.510 (6)	C6–C12	1.503 (6)
C8–C9	1.524 (7)	C10–C11	1.526 (7)
C13–C14	1.522 (7)	C15–C16	1.541 (7)
Bond Angles			
Fe1–O11–Fe1	119.84 (23)	Fe2–O22–Fe2	119.24 (24)
Fe1–O12–Fe2	121.65	Fe1–O21–Fe2	151.23 (19)
O1–Fe1–O3	87.30 (13)	O5–Fe2–O7	88.80 (13)
O1–Fe1–O11	86.09 (13)	O5–Fe2–O22	87.42 (12)
O1–Fe1–O12	89.84 (13)	O5–Fe2–O12	87.65 (12)
O1–Fe1–O21	174.38 (13)	O5–Fe2–O21	174.71 (14)
O1–Fe1–N1	77.04 (13)	O5–Fe2–N2	77.60 (13)
O3–Fe1–O11	97.62 (12)	O7–Fe2–O22	95.35 (12)
O3–Fe1–O12	161.47 (12)	O7–Fe2–O12	160.99 (12)
O3–Fe1–O21	90.06 (14)	O7–Fe2–O21	91.13 (14)
O3–Fe1–N1	73.80 (13)	O7–Fe2–N2	73.89 (13)
O11–Fe1–O12	100.45 (11)	O22–Fe2–O12	103.14 (11)
O11–Fe1–O21	99.19 (13)	O22–Fe2–O21	97.85 (13)
O11–Fe1–N1	161.28 (15)	O22–Fe2–N2	161.54 (15)
O12–Fe1–O21	91.08 (14)	O12–Fe2–O21	90.72 (13)
O12–Fe1–N1	87.72 (14)	O12–Fe2–N2	87.14 (12)
O21–Fe1–N1	97.46 (14)	O21–Fe2–N2	97.31 (14)
Fe1–O1–C9	120.49 (32)	Fe2–O5–Cl14	119.61 (31)
Fe1–13–C11	112.26 (31)	Fe2–O7–Cl16	114.28 (32)
Fe1–N1–C7	110.34 (26)	Fe2–N2–C12	111.56 (26)
Fe1–N1–C8	108.57 (27)	Fe2–N2–C13	108.51 (28)
Fe1–N1–C10	101.70 (26)	Fe2–N2–C15	103.23 (26)
C7–N1–C8	112.29 (24)	C12–N2–C13	111.25 (34)
C7–N1–C10	112.71 (38)	C12–N2–C15	111.52 (38)
C8–N1–C10	110.65 (36)	C13–N2–C15	110.46 (36)
Fe1–O12–C1	118.28 (27)	Fe2–O12–C1	120.07 (27)

(38) Armstrong, W. H.; Spool, A.; Papaefthymiou, G. C.; Frankel, R. B.; Lippard, S. J. *J. Am. Chem. Soc.* **1984**, *106*, 3653–3667.
(39) Wieghardt, K.; Pohl, K.; Gebert, K. *Angew. Chem., Int. Ed. Engl.* **1983**, *22*, 727–728.
(40) Plowman, J. E.; Loehr, T. M.; Schauer, C. K.; Anderson, O. P. *Inorg. Chem.* **1984**, *23*, 3553–3559.

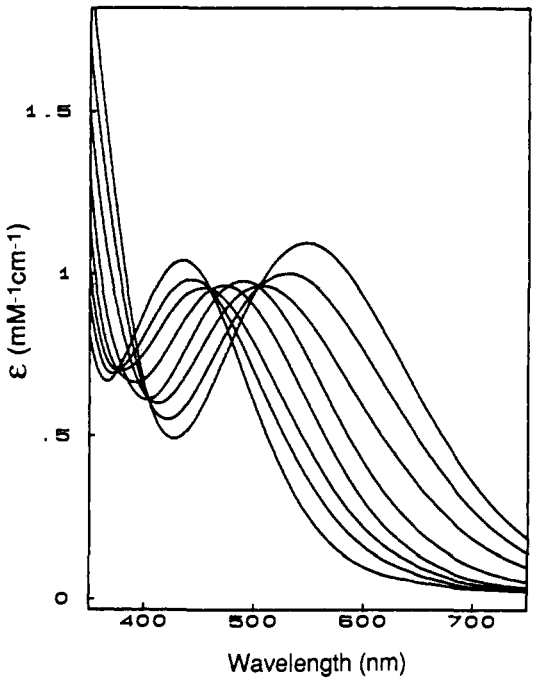

Figure 4. Visible spectra of $[Fe(5\text{-Me-HDA})(H_2O)_2]$ during pH titration. Spectra with absorption maxima from right to left correspond to pH values of 4.66, 5.70, 6.24, 6.97, 8.74, 9.28, 9.62, and 10.24.

in iron(II)–carboxylate complexes.[41] These changes are undoubtedly due in part to the electronic requirements of the iron–oxo bonds, which are thought to have a significant π component. We have earlier noted a similar lengthening of the iron-bridging phenolate bonds in $(sal)_3$trien complexes[31,32] because of the presence of strong iron–terminal phenolate interactions.

The core nuclearity also appears to affect the carboxylate C–O bond lengths. A comparison of the carboxylate C–O bonds in the two complexes shows that these bonds become more similar in length as the Fe–O (carboxylate) bond lengthens. This trend would be consistent with the weakening of the carboxylate interaction with the metal center in the tetranuclear complex due to the presence of Fe–oxo bonds, resulting in a species more like a free carboxylate anion. Thus, the carboxylates in the binuclear complex reflect a structure where the charge is localized, while those on the tetranuclear complex have a more delocalized character. The hydrogen bonding on the uncoordinated oxygens to the pyrrolidinium cations would also contribute to this charge delocalization.

Solution Chemistry of Fe(HDA) Complexes. As a prelude to our study of the iron chemistry of the HXTA ligand, we have investigated the chemistry of its mononucleating analogue, HDA, to serve as a point for comparison. The stoichiometric addition of Fe(III) salts to aqueous solutions of HDA over the range pH 2–10 leads to the formation of deeply colored complexes, which can be isolated from methanol solutions as $FeL(MeOH)_2$. The iron chemistry of the parent HDA ligand in water has been investigated by Martell and co-workers,[21] and we have extended this study to substituted HDAs. The visible spectrum of $[Fe(5\text{-Me-HDA})(H_2O)_2]$ shows a maximum near 550 nm at pH 3.75, which is attributed to a phenolate-to-Fe(III) charge-transfer transition. Figure 4 shows a pH titration for the 5-Me-HDA complex, showing nearly isosbestic behavior as the pH is increased. The two sets of isosbestic points indicate a clean transition from a neutral species to a monobasic form and then onto a dibasic form. Table VI summarizes the data accumulated for the family of HDA complexes. The absorption maximum progressively shifts to higher energies as the pH is increased; this reflects a decrease in the Lewis acidity of the Fe(III) center, as expected for the replacement of an aquo ligand with the more basic hydroxide. The shifts in the absorption band are consistent with our understanding of phenolate-to-Fe(III) charge-transfer transitions.[42] As the substituents on the HDA ligands become more electron donating, the charge-transfer band decreases in energy since these groups would raise the energy of the phenolate orbitals; the pK_a's for the bound water ligands also increase due to the decreased Lewis acidity of the Fe(III) center.

Table VI. Spectral Properties and pK_a's for Fe(HDA) and Fe_2(HXTA) Complexes[a]

	pH	λ_{max}, nm	ϵ, M^{-1} cm^{-1}
Fe(HDA)			
neutral	4.0	522	1120
$pK_1 = 5.7$[b]			
monoanion	7.4	460	1010
$pK_2 = 9.1$[b]			
dianion	10.5	416	1110
$Fe(Cl_2HDA)$			
neutral	3.75	520	1230
$pK_1 = 5.75$			
monoanion	7.40	466	1070
$pK_2 = 9.05$			
dianion	10.5	418	1180
Fe(5-Me-HDA)			
neutral	3.75	550	1100
$pK_1 = 6.5$			
monoanion	7.75	482	980
$pK_2 = 9.4$			
dianion	11.7	432	1040
$Fe(Bu_2HDA)$			
neutral	4.0	482	1280
$pK_1 = 6.5$			
monoanion	8.1	516	1090
$pK_2 = 9.8$			
dianion	11.7	430	1600
Fe_2(5-Me-HXTA)			
neutral	3.0	472	690
monoanion[c]	4.6	446 (sh)	670
dianion	10	350, 550 (sh)	5750, 180
Fe_2(5-Cl-HXTA)			
neutral	2.9	460	740
monoanion[c]	4.4	436 (sh)	740
dianion	10	350, 550 (sh)	5670, 160

[a] Measurements made in 0.1 M NaCl aqueous solution except for Fe_2(5-Cl-HXTA), which was done in 1 M NaCl. [b] Reference 21. [c] Spectrum is concentration dependent.

The NMR spectra of the HDA complexes exhibit paramagnetically shifted features, expected for Fe(III)–phenolate complexes (Table VII). The trend in isotropic shifts observed for the various complexes follows the general trend in charge-transfer energies; the lower the energy of the charge-transfer band, the larger the isotropic shifts observed.[42] pH titrations of $[Fe(HDA)(H_2O)_2]$ monitored by NMR show a progressive decrease of the isotropic shifts observed with an increase of pH, indicative of a facile exchange between the various pH forms of the complex. This suggests that the various pH forms of the commplex are related by simple proton-transfer equilibria, which would be fast on the NMR time scale, i.e.

$$[Fe(HDA)(H_2O)_2] \rightleftharpoons [Fe(HDA)(H_2O)(OH)]^- + H^+ \rightleftharpoons [Fe(HDA)(OH)_2]^{2-} + 2H^+$$

Solution Chemistry of the Fe_2HXTA Complexes. The visible spectrum of $[Fe_2(5\text{-Me-HXTA})OH(H_2O)_2]$ in water shows an absorption maximum near 470 nm, a position blue-shifted relative to the mononuclear Fe(5-Me-HDA) complex. This reflects the lengthening of the iron–phenolate bond due to phenolate bridging two iron centers. A pH titration of $[Fe_2(5\text{-Me-HXTA})OH(H_2O)_2]$, shown in Figure 5, shows the formation of two new complexes as the pH is raised, corresponding to the loss of one and two protons from the parent complex. For the monobasic species, the charge-transfer band blue-shifts and becomes obscured

(41) Chaudhuri, P.; Wieghardt, K.; Nuber, B.; Weiss, J. *Angew. Chem., Int. Ed. Engl.* **1985**, *24*, 778–779.

(42) Pyrz, J. W.; Roe, A. L.; Stern, L. J.; Que, L., Jr. *J. Am. Chem. Soc.* **1985**, *107*, 614–620.

Table VII. Chemical Shifts (Integrations) for the Three Protonation States of Fe(HDA), Fe(5-Me-HDA), and Fe_2(5-Me-HXTA) Complexes

		resonances			
complex	pH	para[a]	meta	benzylic	carboxymethylene
Fe(HDA)	4.6	−74 (1)	81 (1), 52 (1)	n.o.	n.o.
	7.5	−60 (1)	70 (1), 40 (1)	n.o.	n.o.
	11.2	−44 (1)	59 (1), 31 (1)	n.o.	n.o.
Fe(5-Me-HDA)	3.4	93 (3)	82 (1), 53 (1)	n.o.	n.o.
	7.9	72[b]	72[b], 40 (1)	n.o.	n.o.
	11.2	54[b]	58[b], 30 (1)	n.o.	n.o.
Fe_2(5-Me-HXTA)	3.0	55 (3)	51 (2)	n.o.	n.o.
	4.5	27 (3)	32 (1)	4 (1)	8.6 (1)[c], 20 (2)
			20 (1)		123 (1)[c], 163 (1)[c]
	10	8.5 (3)	11.9 (2)	14 (1)[c]	3.5 (2), 8 (2)
				52.5 (2)	20.3 (2), 26.7 (2)

[a] Refers to 5-H of HDA and 5-CH_3 of 5-Me-HDA and 5-Me-HXTA. [b] The 5-Me and 4-H resonances together have an intensity 4 times that of the 6-H. [c] Integration may be low due to broad line width.

by a growing near-UV feature, which is unique to the HXTA complexes. The extinction coefficient of this new feature increases with the concentration of the complex, suggesting the participation of aggregation phenomena. As the dibasic species is formed, a discreet absorption maximum is observed at 350 nm, whose extinction coefficient is concentration independent. A weak shoulder is also observed near 550 nm. The dibasic species corresponds to the tetranuclear complex, $[Fe_4(5\text{-Me-HXTA})_2O_2(OH)_2]^{4-}$, whose structure has been discussed. Similar observations can be made for the corresponding 5-chloro derivative except that the presence of the electron-withdrawing chloro group results in a blue-shift of all the spectra.

The solution behavior of the HXTA complexes is thus somewhat more complex than that for the HDA complexes. Two forms of the Fe_2HXTA complex have been crystallized, a binuclear complex under acidic conditions and a tetranuclear complex under basic conditions. The data we have accumulated (vide infra) indicate that these structures persist in solution at their respective pH's. The pH titration shows the presence of yet another species at intermediate pH; this monobasic intermediate could in principle be binuclear or tetranuclear. Possible structures (**a**–**c**) for the intermediate are shown. Structure **a** corresponds to the ionization

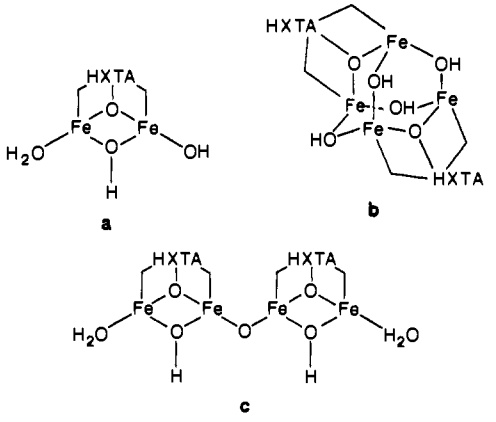

of one of the coordinated aquo ligands in $[Fe_2(5\text{-Me-HXTA})OH(H_2O)_2]$, while structure **b** is derived from the protonation of the oxo groups of $[Fe_4(5\text{-Me-HXTA})_2O_2(OH)_2]^{4-}$. Structure **c** is a plausible alternative to the other two, derived from the dimerization of structure **a** with the loss of a water molecule.

The spectral features of the monobasic intermediate show a concentration dependence. The extinction coefficient of the feature at 350 nm increases as the concentration of the complex increases, suggesting that the intermediate is a result of an associative process, i.e.

$$2A \rightleftharpoons B \qquad K = B/A^2$$

The 350-nm feature appears to be characteristic of both the intermediate and the tetranuclear species; at high concentrations of complex, the maximum absorbance of the interemdiate at 350 nm appears to correspond to half that of the tetranuclear species.

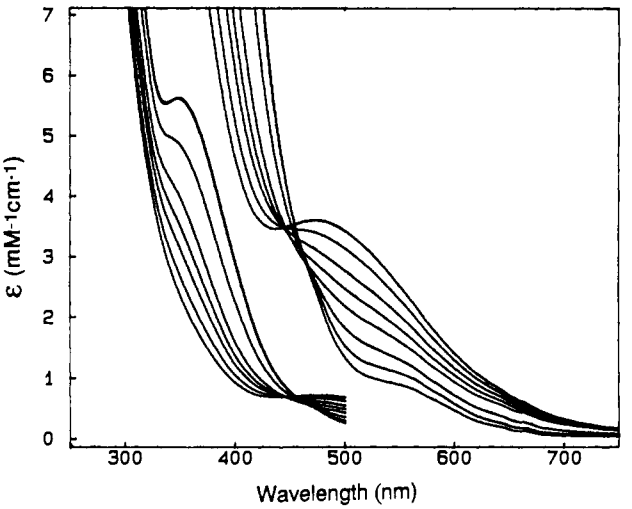

Figure 5. UV–visible spectra of the pH titration of $[Fe_2(5\text{-Me-HXTA})OH(H_2O)_2]$. pH values corresponding to the spectra in order of diminishing absorbance at 500 nm and increasing absorbance at 350 nm: 3.15, 3.46, 3.73, 3.99, 4.66, 5.96, 7.70, 9.90 in 1 M NaCl. Scale for the visible region is $\epsilon/5$.

Table VIII. Concentration Dependence of pK_a's of Fe_2(HXTA) and Association Constants for Dimerization of the Binuclear Forms

	concn, mM	pK_a[a]	log K[b]
Fe_2(5-Cl-HXTA)	0.057	4.0, 5.40	4.1 (1)
	0.57	3.65, 5.3	4.3 (1)
	5.7	3.45, 5.25	4.4 (2)
Fe_2(5-Me-HXTA)	0.2	3.9, 5.9	4.2 (3)
	2.0	3.65, 5.9	4.3 (2)
	10.0	3.55, 6.0	n.d.

[a] Determined at 23 °C in 1 M NaCl; uncertainties in pK_a ± 0.1. [b] Average of at least three determinations.

We have thus used this observation to estimate the concentration of the intermediate species to calculate the approximate association constant. The log K values were determined for both the 5-Me and 5-Cl complexes over a 100-fold concentration range at pH 3.8–4.2 and found to range from 4.2 to 4.4 under the conditions studied (Table VIII). A consequence of the associative equilibrium is the observed concentration dependence of the apparent pK_a's for dissociation of the bound water ligands. This is typical for systems where association of deprotonated species occurs.[43] The above observations would thus seem to indicate that the intermediate would be associated under most of the conditions of investigation and that structure **a** is at best a minor species in solution.

The 350-nm band observed at higher pH's is a feature that has been associated with the presence of iron(III)–oxo bonds in several complexes.[38,40,44,45] Confirmation of their presence in solution

(43) Sillen, L. G. *Q. Rev. Chem. Soc.* **1959**, *13*, 146–168.

Table IX. Resonance Raman Frequencies for Fe_2(5-R-HXTA) Complexes

R	pH	Raman bands							
Me	3.9	421	492	802	1162	1240	1314	1480	1617
	3.9 ($H_2{}^{18}O$)	415	492	802	1162	1240	1314	1480	1617
	10	425	494	804	1164	1252	1313	1480	1618
	10 ($H_2{}^{18}O$)	418	494	804	1164	1252	1313	1480	1618
Cl	10	424			1114	1273	1301	1470	1595
Me, 4,6-d_2	10	425	496		1186	1235	1312	1433	1609
					1196	1251	1385	1470	

[a] 75% deuteriated at the meta protons.

Table X. Correlation of Fe–O–Fe Vibration with Angle in Oxo-Bridged Complexes

complex	$\nu_{Fe-^{16}O-Fe}$, cm^{-1}	$\nu_{Fe-^{18}O-Fe}$, cm^{-1}	∠Fe–O–Fe, deg	ref
$[Fe_4(5\text{-Me-HXTA})_2O_2(OH)_2]^{4-}$	425	418	151.2	this work
$[Fe_4(5\text{-Me-HXTA})_2O(OH)_2(H_2O)_2]^{2-}$	421	415	~151	this work
$[(HB(pz)_3Fe)_2O(OAc)_2]$	528	511	123.6	38
$[(tacnFe)_2O(OAc)_2]^{2+}$	540	523	118.5	51
$[((phen)_2Fe)_2O(H_2O)_2]^{4+}$	395	390	155.1	40
methemerythrin-N_3	507	491	135	4, 52

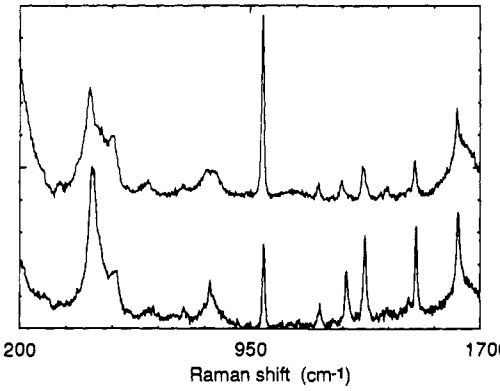

Figure 6. Resonance Raman spectra of $[Fe_2(5\text{-Me-HXTA})OH(H_2O)_2]$ in H_2O at pH 4.0 (upper) and pH 10 (lower) with 457.9-nm excitation. The feature at 983 cm^{-1} arises from the 0.1 M potassium sulfate standard.

is obtained by the observation of resonance-enhanced Raman bands in the 500-cm^{-1} region, associated with the Fe–O–Fe symmetric stretch.[38,40,46,47] The neutral complex shows no feature attributable to an Fe–O–Fe vibration and at best very weak resonance enhancement of the phenolate deformations. However, the intermediate and the tetranuclear species exhibit strongly enhanced spectra containing bands arising from both Fe–O–Fe and phenolate vibrations (Figure 6; Table IX). Both complexes show prominent features around 420, 1160, 1250, 1320, 1480, and 1620 cm^{-1}, all of which are polarized.

The features above 1100 cm^{-1} are assigned to phenolate deformations; these are affected by changing ring substituents and correspond to vibrations observed for other metal–phenolate complexes.[48]

The band near 420 cm^{-1} is affected only by the use of $H_2{}^{18}O$, shifting to lower frequency by 7 cm^{-1} in both the intermediate and the tetranuclear complex. This indicates the incorporation of isotopically labeled solvent molecules and thus allows the assignment of this band to the symmetric Fe–O–Fe stretch. Relative to the 0.1 M sulfate internal standard, this feature shows an enhancement factor of ca. 10 and 20 with 457.9-nm excitation for the intermediate and the tetranuclear complexes, respectively. For comparison, hemerythrin, ribonucleotide reductase, and $[(HB(pz)_3Fe)_2O(OAc)_2]$ exhibit factors of 100–300; $[(tacnFe)_2(OAc)_2]^{2+}$, $[Fe(N\text{-Prsal})_2]_2O$, and $[Fe(HEDTA)]_2O^{2-}$ show factors of 1–20.[49] The complexes under study thus fall into the latter category.

The value for ν_s(Fe–O–Fe) is indicative of the Fe–O–Fe angle. Theoretical calculations have shown that ν_s(Fe–O–Fe) increases as the Fe–O–Fe angle decreases; similarly the extent of isotope shift with ^{18}O increases as the Fe–O–Fe angle decreases.[50] Table X shows a comparison of the Fe–O–Fe data for several (μ-oxo)diiron(III) complexes.[38,40,51,52] On the basis of this table, the HXTA complexes would have an angle slightly smaller than that for $[((phen)_2Fe)_2O(H_2O)_2]^{4+}$. Using the values for ν_s(Fe–O–Fe) from the Raman data and ν_{as}(Fe–O–Fe) from IR spectra of the solid (795 cm^{-1}) and the Fe–O–Fe angle from the crystal structure of $[Fe_4(5\text{-Me-HXTA})_2O_2(OH)_2]^{4-}$, we have determined the force constants, ν_d and ν_{dd}, for the three-body Fe–O–Fe unit to be 3.44 and 0.69 mdyn/Å, respectively. These values predict an ^{18}O isotope shift of 7 cm^{-1} for the symmetric Fe–O–Fe stretch, in accord with the observed shifts. Thus both complexes would appear to have at least one Fe–O–Fe unit with an angle of ca. 150°.

The Raman spectra observed for the two complexes have been obtained with visible excitation (457.9–620 nm); no experiments using near-UV excitation have been attempted. The excitation profiles of both complexes show increasing enhancement of both the Fe–O–Fe and the phenolate bands as the excitation wavelength shifts to the near-UV. The association of the UV–visible spectral features with the excitation profiles in these complexes is not straightforward and is an area that requires further scrutiny.

The NMR spectra of these complexes provide further insight (Figure 7). $[Fe_2(5\text{-Me-HXTA})OH(H_2O)_2]$ exhibits two broad features near 50 ppm in D_2O. The sharper peak at 55 ppm is associated with the 5-Me group, by comparison with the 5-Cl derivative. The broader component near 50 ppm is associated with the meta protons and appears as a single peak in the 5-Cl derivative. An unidentified minor species is also detected with a single resonance at 23 ppm; the intensity of this peak varies with conditions and is greatly diminished in the 5-Cl derivative when studied under the same conditions.

The shift of the methyl group in $[Fe_2(5\text{-Me-HXTA})OH(H_2O)_2]$, 55 ppm, is substantially diminished relative to that of $[Fe(5\text{-Me-HDA})(H_2O)_2]$, 89 ppm, at the same pH. Two factors contribute to this large difference. The phenolate-to-Fe(III) charge-transfer transition occurs at higher energy for the binuclear complex and thus results in the delocalization of less unpaired spin density onto the HXTA ligand.[42] A more valid comparison can be made with $[Fe(5\text{-Me-HDA})(H_2O)(OH)]^-$, which has the

(44) Spiro, T. G.; Saltman, P. *Struct. Bonding (Berlin)* **1969**, *6*, 116–156.
(45) Schugar, H. J.; Rossman, G. R.; Barraclough, C. G.; Gray, H. B. *J. Am. Chem. Soc.* **1972**, *94*, 2683–2690.
(46) Shiemke, A. K.; Loehr, T. M.; Sanders-Loehr, J. *J. Am. Chem. Soc.* **1984**, *106*, 4951–4956.
(47) Sjöberg, B.-M.; Loehr, T. M.; Sanders-Loehr, J. *Biochemistry* **1982**, *21*, 96–102.
(48) Que, L., Jr. *Coord. Chem. Rev.* **1983**, *50*, 73–108.
(49) Sanders-Loehr, J., personal communication.
(50) Wing, R. M.; Callahan, K. P. *Inorg. Chem.* **1969**, *8*, 871–874.
(51) Spool, A.; Williams, I. D.; Lippard, S. J. *Inorg. Chem.* **1985**, *24*, 2156–2162.
(52) Freier, S. M.; Duff, L. L.; Shriver, D. F.; Klotz, I. M. *Arch. Biochem. Biophys.* **1980**, *205*, 449–463.

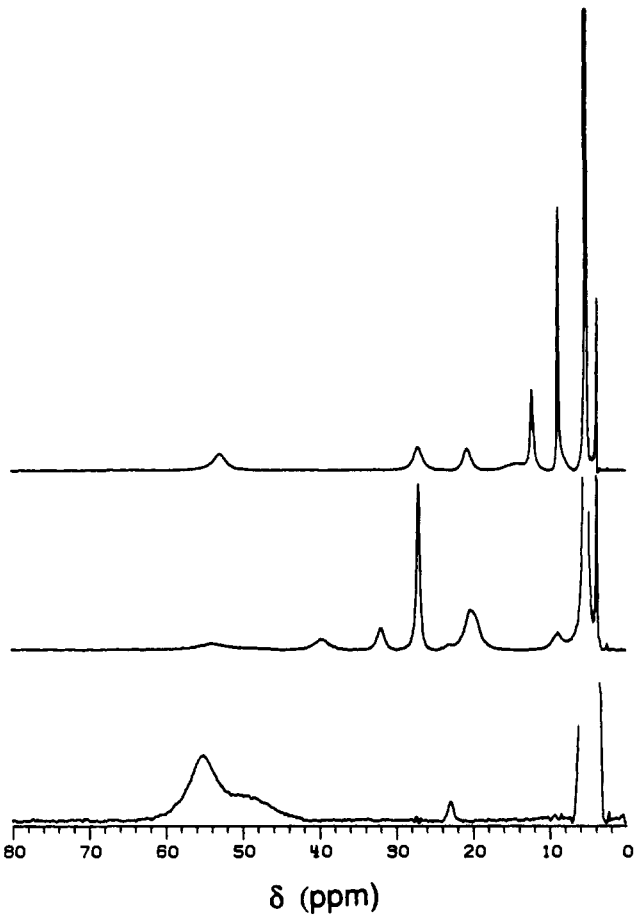

Figure 7. ^1H NMR spectra of $[Fe_2(5\text{-Me-HXTA})OH(H_2O)_2]$ at pH 3 (bottom), 4.3 (middle), and 9 (top). pH uncorrected for D_2O solvent.

same absorption maximum as $[Fe_2(5\text{-Me-HXTA})OH(H_2O)_2]$; the methyl shift for the mononuclear complex is still larger (70 ppm). The added decrease is due to the antiferromagnetic coupling between the iron centers via the phenolate and hydroxide bridges that decreases the magnetic susceptibility of the binuclear complex relative to the mononuclear complex. The value for the antiferromagnetic coupling for $[Fe_2(5\text{-Me-HXTA})OH(H_2O)_2]$ has been estimated to be ca. -11 cm^{-1} from the temperature dependence of the isotropic shifts (Figure S2, supplementary material),[53] in agreement with variable-temperature solid-state susceptibility data (vide infra).

Upon stepwise addition of 1 equiv of base to $[Fe_2(5\text{-Me-HXTA})OH(H_2O)_2]$, its peaks shift 1–2 ppm upfield and then diminish greatly in intensity. During this addition, a new set of peaks appears at 40, 31, 27, and 20 ppm with an intensity ratio of 1:1:3:3, increasing in intensity as the pH is increased; an additional peak at 8 ppm of uncertain intensity is also detected. These peaks correspond to the intermediate complex and are in slow exchange with those of the binuclear complex. The new features have been assigned by comparison with the spectra of deuteriated analogues and the 5-Cl derivative (Table VII). The 5-Me resonance is observed at 27 ppm, while the meta protons appear as two peaks at 31 and 20 ppm from the ^2H NMR of the meta-deuteriated intermediate complex. Thus the HXTA ligand in the intermediate complex appears to have lost its C_2 symmetry.

In contrast to the observation in aqueous solution, the addition of base to $[Fe_2(5\text{-Me-HXTA})OH(H_2O)_2]$ in dry methanol results in a smooth shift of the 5-Me resonance upfield, and no new peaks are observed. The shift of the methyl resonance is reminiscent of the behavior of the Fe(HDA) complexes and indicates a rapid equilibrium between the binuclear complex and its conjugate base. The differences in the behavior of the monoanionic species in the two solvents can be rationalized in terms of the associative equilibrium discussed earlier. At 5–10 mM complex in water, the association constant predicts that the binuclear complex would be >90% associated.

The addition of another 1 equiv of base to the binuclear complex results in the appearance of a third set of peaks, assigned to the tetranuclear complex, which are in slow exchange with the peaks of the intermediate complex. The isotropic shifts observed are the smallest of the three complexes and consistent with strong antiferromagnetic coupling expected for the two oxo bridges in the molecule. The meta protons are equivalent, indicating that the HXTA ligand has regained its C_2 symmetry. There are four carboxymethylene resonances; because of the three approximate C_2 axes in the molecule, the four resonances are interpreted to result from the four hydrogens of one (*N*-carboxymethyl)glycine portion of the ligand. The range of shifts observed for the carboxymethylene protons reflects the variation in geometry of the C–H bond relative to the Fe–N bond, the magnitude of the isotropic shift being quantitatively dependent on dihedral angle.[54] On the basis of this relationship, the protons with the largest and smallest isotropic shifts can probably be assigned to one carbon and the protons with the intermediate shifts to the other. The average positions of these two sets are quite similar by this assignment (15.1 and 14.1 ppm), but are much smaller than the average shifts of the benzylic protons (33 ppm). The paramagnetic shifts for these protons are expected to be a sum of contributions from spin delocalization via the Fe–N bond and the Fe–OOC bond (for the carboxymethylenes) or the Fe–phenolate bond (for the benzylic protons). The difference in the shifts thus reflects the different contributions to the shift of the phenolate or the carboxylate. The phenolate contribution would be similar to the isotropic shift of the 5-Me group (6–7 ppm downfield). This value cannot account for the entire difference and suggests that monodentate carboxylates may contribute an upfield component to the total shift. Such a contribution has been noted for Ni(II) amino acid complexes for carboxymethylene protons.[55,56] The upfield shift for monodentate carboxylates contrasts the large downfield observed for bidentate carboxylates in Fe(III) complexes; this suggests that different delocalization mechanisms may be operative for monodentate and bidentate carboxylates.[57]

The NMR properties of the intermediate complex when compared to those of the binuclear and the tetranuclear complexes indicate that the ligand has lost its C_2 symmetry. This would be inconsistent with structure **b**. The appearance of a new set of peaks associated with the intermediate complex in slow exchange with both the binuclear and the tetranuclear complexes, together with the association equilibria observed in the visible spectra, would eliminate structures **a** and **b** as possibilities. This leaves structure **c**, which is thus far consistent with all the observations. Further support for this is found in magnetic susceptibility measurements and Mössbauer spectra.

The solid-state magnetic moment of $[Fe_2(5\text{-Me-HXTA})OH(H_2O)_2]$ at room temperature is 5.07 (5) μ_B/Fe, a value somewhat reduced from the normal high-spin Fe(III) value of 5.92 μ_B. A similar magnetic moment is observed in solution, 5.0 (1) μ_B/Fe, as measured by the Evans' method. Variable-temperature solid-state susceptibility measurements (Table S7; Figure S4) show the presence of weak antiferromagnetic coupling between the iron(III) centers, with $J = -12$ cm^{-1}. This J value agrees with that estimated from the temperature dependence of the 5-Me isotropic shift (Figure S2) and those observed for other binuclear iron(III) complexes with a phenolate and a hydroxide bridge.[31]

The solid-state magnetic moment for $[Fe_4(5\text{-Me-HXTA})_2O_2(OH)_2]^{4-}$ at room temperature is 1.74 μ_B/Fe, indicative of strong antiferromagnetic coupling via the oxo bridges. The

(53) Maroney, M. J.; Kurtz, D. M., Jr.; Nocek, J. M.; Pearce, L. L.; Que, L., Jr. *J. Am. Chem. Soc.* **1986**, *108*, 6871–6879.

(54) Ho, F. F.-L.; Reilley, C. N. *Anal. Chem.* **1969**, *41*, 1835–1841.

(55) Milner, R. S.; Pratt, L. *Discuss. Faraday Soc.* **1962**, *34*, 88–95.

(56) Holm, R. H.; Hawkins, C. J. In *NMR of Paramagnetic Molecules*; La Mar, G. N., Horrocks, W. deW., Jr., Holm, R. H., Eds.; Academic: New York, 1973; pp 243–332.

(57) Arafa, I. M.; Goff, H. M.; David, S. S.; Murch, B. P.; Que, L., Jr. *Inorg. Chem.* **1987**, *26*, 2779–2783.

Table XI. Mössbauer Parameters for Fe_2(5-Me-HXTA) Complexes

complex	conditions	δ,[a] mm/s	ΔE_Q,[a] mm/s	Γ,[a] mm/s	rel intens,[a] %
Fe_2(5-Me-HXTA)OH$(H_2O)_2$	solid	0.50	0.60	0.27	100
$(Me_4N)[Fe_2$(5-Me-HXTA)$(OAc)_2]$	solid	0.49	0,58	0.28	100
$(pyrrH)_4[Fe_4$(5-Me-HXTA)$_2O_2(OH)_2]$	solid	0.52	1.73	0.29	100
Fe_2(5-Me-HXTA)	in solution				
	pH 2.71	0.50	0.67	0.40	100
	pH 3.03	0.50	0.65	0.42	100
	pH 3.5	0.49	0.70	0.42	61
		0.51	1.66	0.42	39
	pH 3.90	0.48	0.73	0.33	52
		0.50	1.79	0.37	48
	pH 4.25	0.48	0.73	0.29	47
		0.50	1.81	0.35	53
	pH 4.6	0.48	0.72	0.27	44
		0.50	1.80	0.34	56
	pH 9.9	0.51	1.65	0,31	100
Fe(HEDTA)[c]		0.69	0.83		
$enH_2[Fe_2$(HEDTA)$_2O]$[c]		0.74	1.75		
Na[Fe(EDTA)][c]		0.73	0.76		
$Na_2[Fe_2$(EDTA)$_2O]$[c]		0.70	1.94		
$[(FeHB(pz)_3)_2O(OAc)_2]$[d]		0.52	1.60		

[a] Uncertainties are ±0.02 mm/s, 0.03 mm/s, 0.02 mm/s, and 3%, respectively. [b] Isomer shift, relative to iron foil at room temperature, except where noted otherwise. [c] Reference 45; isomer shift at 77 K, relative to sodium nitroprusside. [d] Reference 38.

NMR spectrum also reflects the large value of J in solution, manifested by small isotropic shifts and anti-Curie temperature dependence. Variable-temperature magnetic susceptibility measurements are now in progress to sort out the different values for J across the oxo, hydroxo, and phenoxo bridges.

The magnetic susceptibility of the intermediate complex can only be characterized in solution. Evans' susceptibility measurements at pH 4.1–4.7 show a magnetic moment of ca. 3.8 μ_B/Fe, a value that is an average of those for the binuclear and the tetranuclear complexes. A variable-temperature study of the NMR shifts shows Curie behavior for phenolate resonances and anti-Curie behavior for the observable carboxymethylene and benzylic peaks (Figure S3). This behavior would be consistent with structure **c**. The observable methylene resonances arise from protons associated with oxo-bridged iron centers. Their temperature dependences should reflect the strong coupling between those iron centers. The phenolate is coordinated to a metal center that is highly paramagnetic and one that is substantially less so, and the temperature dependences reflect the more paramagnetic center.

Mössbauer studies also confirm the assignment of the intermediate complex to structure **c** (Figure 8; Table XI). All three complexes of 5-Me-HXTA exhibit similar values for the isomer shift, δ, ca. 0.50 mm/s, a value typical of a high-spin Fe(III) center in a non-sulfur environment.[58,59] The presence of an oxo bridge in an Fe(III) complex is often indicated by a large value for ΔE_Q.[38] Thus, $[Fe_2$(5-Me-HXTA)OH$(H_2O)_2]$ exhibits a small ΔE_Q, while $[Fe_4$(5-Me-HXTA)$_2O_2(OH)_2]^{4-}$ exhibits a large ΔE_Q. At the pH where the intermediate complex would be expected to be maximally formed, the Mössbauer spectrum shows evidence for two types of iron centers, one with a small ΔE_Q and the other with a large ΔE_Q, in agreement with the proposed structure. The variations in the relative intensities of the quadrupole doublets at intermediate pH values reflect the presence of the low-pH or high-pH forms in addition to the intermediate complex.

Summary and Perspectives. The observations that we have made in the foregoing discussion indicate that $[Fe_2$(5-Me-HXTA)OH$(H_2O)_2]$ and $[Fe_4$(5-Me-HXTA)$_2O_2(OH)_2]^{4-}$ retain their solid-state structures in solution. These two complexes interconvert in solution depending on the pH via an intermediate complex. On the basis of its UV-visible, resonance Raman, NMR, magnetic susceptibility, and Mössbauer properties, we conclude that the intermediate species is a tetranuclear complex consisting of two Fe_2(5-Me-HXTA) units linked together by an oxo bridge

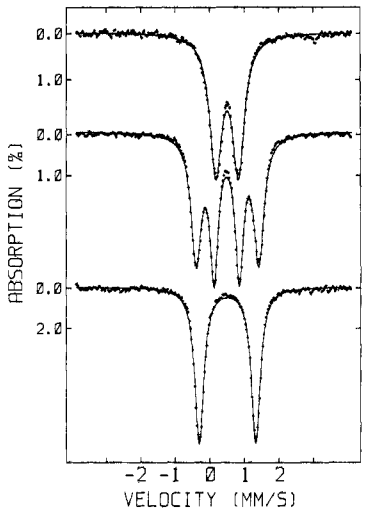

Figure 8. Mössbauer spectra (4.2 K) of $[^{57}Fe_2$(5-Me-HXTA)OH$(H_2O)_2]$ solutions at pH 3.0 (top), 4.3 (middle), and 9.9 (bottom).

(structure **c**). Thus, the two internal iron centers are strongly coupled to each other antiferromagnetically, and they are each in turn coupled weakly to a terminal iron center. Such a linear arrangement of four iron centers is yet another permutation for aggregating four iron atoms via oxo and/or hydroxo bridges.

The intermediacy of structure **c** in the conversion of $[Fe_2$(5-Me-HXTA)OH$(H_2O)_2]$ to $[Fe_4$(5-Me-HXTA)$_2O_2(OH)_2]^{4-}$ raises intriguing questions regarding the factors that promote the oligomerization of iron(III). While $[Fe_2$(5-Me-HXTA)OH$(H_2O)_2]$ readily forms oxo bridges upon dissociation of its water protons, the related mononuclear Fe(HDA) complex retains its mononuclear character even in its dibasic form. The principal difference between the iron-ligand environments provided by 5-Me-HXTA and 5-Me-HDA is that the phenolate is shared by the two iron centers in the binuclear complex. This results in the lenghtening of the Fe–OPh bond and renders the iron centers in the binuclear complex more Lewis acidic relative to the iron center in the HDA complex. The tendency to oligomerize thus appears to be related to the Lewis acidity of the iron(III) center; perhaps this has to do with the accessibility of the iron t_{2g} orbitals for π interaction with the potential oxo ligands. This is borne out, in general, in other iron(III) complexes; i.e., the more Lewis acidic the metal center (as indicated by the pK_a's of the bound water), the greater the tendency to form oxo bridges.

Further oligomerization to form larger aggregates is not possible for the HXTA complexes, because the multidentate ligand oc-

(58) Greenwood, N. N.; Gibb, T. C. *Mössbauer Spectroscopy*; Chapman & Hall: London, 1971; pp 148–168.
(59) Murray, K. S. *Coord. Chem. Rev.* **1974**, *12*, 1–35.

cupies four of the six available sites for each iron. It seems clear that making more sites available will lead to larger aggregates, as in the case of the tridentate tacn ligand, which gives rise to an octanuclear complex,[18] and in the case of the bidentate benzoate, which gives rise to an undecanuclear species.[19] The isolation and structural characterization of these iron-oxo aggregates further enhance our understanding of the core nucleation process in ferritin and the bioinorganic chemistry of rust.

Acknowledgment. This work was supported by the National Institutes of Health Grants GM-33162 (L.Q.) and GM-22701 (Eckard Münck). L.Q. thanks the Alfred P. Sloan Foundation for a Research Fellowship (1982-1986) and the National Institutes of Health for a Research Career Development Award (1982-1987). We thank Professor S. J. Lippard and R. L. Rardin for generously providing and analyzing the variable-temperature susceptibility data on $[Fe_2(5\text{-Me-HXTA})OH(H_2O)_2]$.

Supplementary Material Available: Listings of H atom and solvent atom parameters, temperature factors, and appropriate least-squares planes for $[Fe_2(5\text{-Me-HXTA})OH(H_2O)_2]$ and $(pyrrH)_4[Fe_4(5\text{-Me-HXTA})_2O_2(OH)_2]$ (Tables S1-S6), variable-temperature solid-state susceptibility data on $[Fe_2(5\text{-Me-HXTA})OH(H_2O)_2]$ (Table S7), cation-anion packing in $(pyrrH)_4[Fe_4(5\text{-Me-HXTA})_2O_2(OH)_2]$ (Figure S1), temperature dependences of the NMR signals of $[Fe_2(5\text{-Me-HXTA})]$ complex at pH 3 and 4.3, respectively (Figures S2 and S3), and variable-temperature solid susceptibility data on $[Fe_2(5\text{-Me-HXTA})OH(H_2O)_2]$ and the best fit (Figure S4) (18 pages). Ordering information is given on any current masthead page.

Neutral Bimetallic Macrocyclic Complexes. 1. Investigation of Mono- and Bimetallic Complexes of Tetraiminato Macrocyclic Complexes Derived from 1,3,5-Triketones

M. Himmelsbach, R. L. Lintvedt,* J. K. Zehetmair, M. Nanny, and M. J. Heeg

Contribution from the Department of Chemistry, Wayne State University, Detroit, Michigan 48202. *Received April 16, 1987*

Abstract: The first bimetallic complex of the macrocyclic ligand derived from 1,3,5-triketones and diamines has been synthesized and characterized by single-crystal X-ray diffraction and NMR spectroscopy. It has been determined that the mono- and bimetallic Ni(II) complexes of the macrocyclic ligand formed from ethylenediamine and 2-methyl-3,5,7-octanetrione, $NiH_2(IAA)_2(EN)_2$ and $Ni_2(IAA)_2(EN)_2$, are isomorphous. Both crystallize in the space group $P2_1/c$ ($Z = 2$). For the green platelets of $NiH_2(IAA)_2(EN)_2$: $a = 12.730$ (6), $b = 7.625$ (2), $c = 12.113$ (4) Å; $\beta = 111.40$ (3)°; $V = 1094.8$ (7) Å^3. For the purple platelets of $Ni_2(IAA)_2(EN)_2$: $a = 12.556$ (3), $b = 7.587$ (1), $c = 12.143$ (1) Å; $\beta = 111.09$ (1)°; $V = 1079.2$ (3) Å^3. The bimetallic $Ni_2(IAA)_2(EN)_2$ is highly planar with a Ni-Ni distance of 2.859 (2) Å and angles Ni-O-Ni and O-Ni-O of 101.0 (2)° and 79.0 (2)°, respectively. The structure was also determined for a crystalline disordered mixture of the above mono- and bimetallic products and yielded an average formula $Ni_{1.6}H_{0.8}(IAA)_2(EN)_2$. This structure is isomorphous, with the pure components giving the following cell parameters: $a = 12.646$ (12), $b = 7.609$ (5), $c = 12.131$ (8) Å; $\beta = 111.23$ (6)°; $V = 1088$ (1) Å^3; $Z = 2$. The free ligand, $H_4(IAA)_2(EN)_2$, crystallizes as pale yellow rhombic crystals with space group $C2/c$: $a = 17.649$ (2), $b = 11.036$ (1), $c = 11.659$ (1) Å; $\beta = 97.375$ (8)°; $V = 2251.0$ (4) Å^3; $Z = 4$. Several new macrocylic ligands and their complexes have been prepared and characterized with a Ni(II) template reaction for the triketone-diamine condensation. This includes condensation of benzoyl groups, yielding products that are not accessible except through the template reaction.

The behavior of bimetallic complexes can, in principle, be quite distinct from their monometallic analogues. If metal-metal bonding occurs, the reactivity of this functional group may dominate the observed chemistry. In the absence of metal-metal bonding, characteristic behavior may stem from electronic communication through bridging ligands and/or the spatial proximity of the metal ions. It has been a long-standing interest in this group to examine the properties of bimetallic complexes of triketonate ligands I.[1] In these complexes the metals are maintained by the

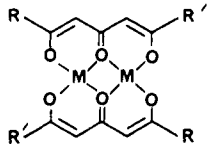

I

rigid backbone at a distance that does not permit metal-metal bonding. The metals still interact, however, as the magnetic data indicate; they are antiferromagnetically coupled through the bridging ligands.[2]

Another means of developing bimetallic chemistry is through the use of a macrocyclic ligand that incorporates two binding sites. The first example of a ligand of this type was reported by Pilkington and Robson in 1970.[3] Condensation of 2-hydroxy-5-methylisophthalaldehyde and 1,3-diaminopropane and loss of the acidic phenolic protons result in a dianionic ligand, which upon complexation with divalent metal ions yields dicationic, bimetallic macrocyclic complexes II. The dicopper complex of II and the

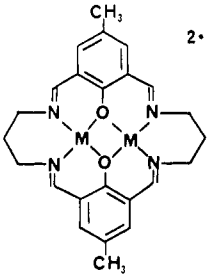

II

(1) (a) Lintvedt, R. L.; Ahmad, N. *Inorg. Chem.* **1982**, *21*, 2356. (b) Heeg, M. J.; Mack, J. L.; Glick, M. D.; Lintvedt, R. L. *Inorg. Chem.* **1981**, *20*, 833. (c) Guthrie, J. W.; Lintvedt, R. L.; Glick, M. D. *Inorg. Chem.* **1980**, *19*, 2949. (d) Kuszaj, J. M.; Tomlonovic, B.; Murtha, D. P.; Lintvedt, R. L.; Glick, M. D. *Inorg. Chem.* **1973**, *12*, 1297.

(2) Glick, M. D.; Lintvedt, R. L. *Prog. Inorg. Chem.* **1976**, *21*, 233.
(3) Pilkington, N. H.; Robson, R. *Aust. J. Chem.* **1970**, *23*, 2225.

0002-7863/87/1509-8003$01.50/0 © 1987 American Chemical Society